Spin spiral and topological Hall effect in Fe_3Ga_4

Mahdi Afshar and Igor I. Mazin

Department of Physics and Astronomy and Quantum Science and Engineering Center, George Mason University, Fairfax, Virginia 22030, USA

(Received 18 May 2021; revised 14 July 2021; accepted 9 August 2021; published 14 September 2021)

A new mechanism for the topological Hall effect (THE) was recently proposed for the spiral magnet YMn_6Sn_6, which requires transverse conical spiral magnetism, induced by external magnetic field, combined with thermally excited helical spiral magnons. In principle, this mechanism should be applicable to other itinerant spiral magnets as well. In this paper, we show that another magnetic compound, Fe_3Ga_4, in which THE was observed experimentally before, in one of its phases satisfies this condition, and the proposed theory of thermal-fluctuation-driven THE is quantitatively consistent with the experiment. This finding suggests that this mechanism is indeed rather universal, and the effect may have been observed in other compounds before but overlooked.

DOI: 10.1103/PhysRevB.104.094418

I. INTRODUCTION

For the past few decades, topological effects driven by magnetic textures have attracted considerable interest [1–5]. In particular, the Hall effect has been widely used as a probe for topological effects. In the classical Hall effect, discovered more than a century ago, the Lorentz force resulting from an external magnetic field gives rise to an electric field perpendicular to the electron current. The theory of this phenomenon is well known and stipulates that the effect is linear in the magnetic field, with the ordinary Hall resistivity $\rho^O = R_0 H$ (the proportionality coefficient R_0 depends on the details of the Fermi surface). In systems with broken time-reversal symmetry (for instance, in ferromagnets), there exists another contribution to the off-diagonal resistivity, dubbed the "anomalous Hall effect" (AHE), $\rho^A = R_s M$. This contribution is proportional to the magnetization M and gives rise to a Hall effect even in the absence of an externally applied magnetic field. While this relation is not always true, for instance, it is violated in some antiferromagnets [6], it has been routinely used to identify the AHE in the experiment.

Very recently, an additional mechanism generating off-diagonal resistivity in magnets with noncoplanar moments was identified [2,7]. Interestingly, contrary to the AHE, this mechanism does not require spin-orbit interaction, although it can benefit from the latter [8]. This mechanism, often called the topological Hall effect (THE), is based on the Berry phase an electron acquires when its spin follows a spatially varying magnetization that is present in such materials. It was shown that its amplitude is proportional to the so-called scalar spin chirality (SSC), defined as the triple product of three spins forming a triangle:

$$\Omega = \mathbf{S}_1 \cdot (\mathbf{S}_2 \times \mathbf{S}_3). \tag{1}$$

In principle, this mechanism is not supposed to work in a system with zero SSC and weak spin-orbit coupling (as in many $3d$ metals). Yet in several cases sizable deviations from the standard formula, $\rho = \rho^O + \rho^A = R_o H + R_s M$, were reported [9–12] and ascribed to THE, even though for all these systems the magnetic structure is known and does not have any SSC.

For one of these compounds, namely, YMn_6Sn_6, a particularly detailed set of experimental data was available [10], and another mechanism for THE was proposed. Within this scenario, SSC emerges through a fluctuational mechanism akin to the emerging nematicity in an Fe-based superconductor [13]. The resulting THE amplitude grows roughly linearly with temperature, with a quadratic dependence on magnetization. The prerequisites to this fluctuational THE (FTHE) are (a) a transverse conical spiral magnetic state at least in some range of temperatures and external fields, (b) itinerant electrons strongly coupled with this spiral (ideally, formed by the same electron orbitals), and (c) strong fluctuations.

In this paper, we will study another compound in which THE has been reported [9], Fe_3Ga_4, and will show that this observation is consistent with the same FTHE mechanism. In the following section we will describe the compound and the experimental picture; then we will present the results of our density functional theory (DFT) calculations and discuss the magnetic phase diagram. After that, we will review the theory of the FTHE and apply it to Fe_3Ga_4.

II. EXPERIMENTAL SITUATION

Fe_3Ga_4 crystallizes in a base-centered monoclinic structure, with the symmetry group $C2/m$, and a rather complex primitive unit cell of 3 f.u. The four crystallographically inequivalent Fe sites form seven parallel sheets along the c direction, as shown in Fig. 1, with interlayer distances of 0.368, 1.334, 1.104, 1.104, 1.334, 0.368, and 0.977 Å. The lattice parameters are $a = 10.0979$ Å, $b = 7.6670$ Å, and $c = 7.8733$ Å, with an obtuse angle of $\beta = 106.298^\circ$ [9]. While crystallographically and electronically, as will be discussed in more detail later, it is rather three-dimensional (3D),

 ©2021 American Physical Society

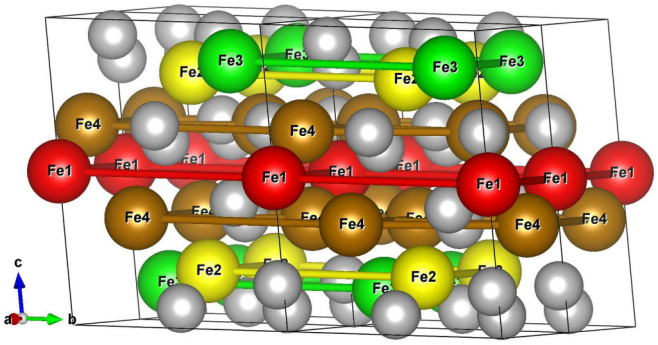

FIG. 1. Layered structure of Fe atoms in Fe_3Ga_4 crystal structure (plotted using the VESTA package [15]). The four different crystallographically inequivalent iron sites are shown in different colors. There are also four unique Ga sites, which are all shown in gray.

magnetically, it can be viewed as a stack of ferromagnetically ordered planes with complex, but, presumably, weaker, interplanar coupling [14].

The material is known to have two magnetic transitions [9,14], from a ferromagnetic (FM) to a spin density wave (SDW) at $T_1 = 60$ K and back to a ferromagnetic state at $T_2 \approx 360$ K [in this paper we apply the term SDW to any phase where spin polarization varies periodically in space; thus defined, SDW can be either a spin spiral (SS) or an *amplitude* spin density wave (ASDW), wherein the magnitude of the magnetic moment varies continuously, or a combination of both]. The long-range order is lost at $T_3 = 420$ K. The nature of the SDW phase will be discussed later; we will just mention that the neutron data can be fit equally well [14,16] by an ASDW, where the spins are mostly aligned along a, or by a spin spiral with the helical orientation, i.e., with the spins rotating in the ab plane. Either way, the spiral wave vector appears to be (0,0,0.29) at $T = 100$ K and gradually reduces after ≈200 K to (0,0,0.25) at room temperature. The low-T and high-T phases are identified as ferromagnetic, although the high-T phase may be a noncollinear canted phase with non-zero net magnetization. In this paper, however, we will not be concerned with the natures of those phases, only with the SDW phase between T_1 and T_2.

Experimentally, the neutron scattering experiments [14] indicate that in the low-temperature ferromagnetic phase the moments are oriented along c, suggesting that c is the magnetic easy axis in this temperature range. In the SDW phase (see Ref. [14], Fig. 3(a), for the data at $T = 100$ K), in the low field (<0.3 T) the spin susceptibility is the lowest for the field direction along a and the highest along c, but the c and b directions are nearly the same. In this $C2/m$ structure the c axis forms a slightly obtuse angle of 105.8° with a, so that formally, a small off-diagonal anisotropy is allowed and the principal magnetic axes may deviate from the crystallographic axes. This effect is likely small, and in the following qualitative discussion we neglect the difference between the magnetic and crystallographic axes. If this SDW is assumed to be approximately collinear [14,16], the hierarchy of the spin suceptibilities would imply that a is the easy axis and b and c are the hard ones, with b being slightly harder. This assignment is consistent with the first neutron structure, an amplitudinal wave mostly polarized along a. Note that this structure implies that the easy axis rotates from c to a in this temperature range. In higher fields a spin-flip (not spin-flop) transition into a ferromagnetic state with $M \gtrsim 3\mu_B$/f.u. is observed. For the field direction b it happens at $H \approx 5$ T, and for the fields along a or c at a much higher field, $H \approx 7$ T. In an ideally collinear antiferromagnet (the amplitude SDW proposed in Ref. [14] is rather close to that) the spin-flip field is the lowest along the easy axis and the hardest along the hardest axis (since Zeeman energy in this case needs to overcome an additional loss of the magnetic anisotropy energy). Thus, from the spin-flip data at 100 K we have to conclude that b is the easy axis, and a and c are approximately equally hard, in obvious contradiction not only to the low-T FM spin orientation but also to the fact that spins in the assumed ASDW state at the same temperature lie predominantly along a.

On the other hand, if we assume that the magnetic state at $T = 100$ K is an *ab-helical* spin spiral, then c must be the hardest axis. This assignment is consistent with the fact that the low-field susceptibility is the highest along c, for a conical spiral is normally preferred over a planar-distorted one. From the differences between the in-plane susceptibility it follows that in this case b is the easier axis of the two.

In Table I we list the anisotropies consistent with the experiment and the two alternative interpretations of the SDW phase. We can see that regardless of the accepted interpretation, the anisotropy at $T = 100$ K disagrees with the low-temperature data. On the other hand, the anisotropies deduced from the spin-flip field and from the susceptibility are inconsistent with each other in the ASDW scenario but are consistent in the SS one. That is to say, contrary to the assumption in Ref. [14], the latter is *more*, not *less*, consistent with the entire set of experimentally measured anisotropies at $T = 100$ K.

At $T = 100$ K there are no other detectable phase transitions, implying that at this temperature the SDW state bypasses a spin-flop and immediately transitions into a forced-ferromagnetic state via a spin flip. On the other hand, magnetometry at higher temperatures, $\gtrsim$150 K, suggests the possibility of a spin-flop transition at very low fields $H \lesssim 0.1$ T for $H \perp c$ [9]. This fact is consistent with both an ab helical spiral and an a polarized ASDW. Had magnetometry data resolved in the ab plane been available, one could distinguish between the two scenarios because the spin flop is expected for both a and b in the former case but only for a in the latter.

The residual resistivity was relatively large, with the room-temperature ratio ∼2, indicating a large number of defects and possibly deviations from stoichiometry. The residual specific heat coefficient $C(T)/T|_{T\to 0} = 23$ mJ/mole K^2, corresponding to the density of states (DOS) at the Fermi level $N(0) \approx 10$ states/f.u. Only the first phase transition, at $T = T_1$, has a distinct specific heat signature, and the entropy change is very small, less than 0.3% of Rln2, indicating that the transition occurs between two well-ordered states. The authors of Ref. [9] estimated that entropy change between T_2 and T_3 as 0.43 J/mole K, which is less than 10% of Rln2, consistent with a quasi-two-dimensional character of magnetism in this material.

Transport measurements indicate an extra contribution for the Hall effect ρ_{xy} (i.e., in a magnetic field in the ab plane) for

an intermediate temperature range, roughly coinciding with the (T_1, T_2) interval, compared with the standard combination of anomalous and ordinary Hall effects,

$$\rho_{xy}(H) = R_o H + R_s M. \tag{2}$$

The coefficients R_o and R_s strongly depend on the phase and, inside each phase, also depend on temperature, which makes it difficult to quantify the additional, presumably topological, contribution, but one can say with confidence that this contribution increases with temperature up to the highest reported temperature of 350 K.

III. DFT CALCULATIONS

Calculations of the structural, electronic, and magnetic properties of bulk Fe_3Ga_4 were performed using the Vienna Ab initio Simulation Package (VASP) [17–20]. Fe $3s$, $3p$, $3d$, and $4s$ and Ga $3p$, $3d$, and $4s$ states were treated as valence. The plane cutoff was 500 eV. We use Gaussian smearing with a width of 0.05 eV, with this value ensuring an entropy contribution to the free energy of less than 1 meV/atom. The generalized gradient approximation (GGA) was used for the exchange-correlation functional [21]. The spin-orbit coupling was included in the self-consistent calculations, unless specified otherwise. The k-point sampling was based on a Γ-centered grid for all calculations, and we used an optimized $(10 \times 10 \times 10)$ k-point grid, except for the DOS calculations, where the $12 \times 12 \times 9$ grid was utilized.

In addition, we used the all-electron Full-Potential Local Orbitals (FPLO) [22] package, which solves the fully relativistic Dirac equations [23]. The basis set included Fe $(1s, 2s, 2p, 3s, 3p, 3d)$ and Ga $(3s, 3p, 3d, 4s, 4p, 4d, 5s)$ states. The total energy converged to 0.001 meV. In order to address the possible effect of the on-site electron correlations, we employed the GGA+U method in the fully localized limit [24]. As implemented in FPLO, it has full nonspherical double-counting subtraction (as opposed to most other codes), whereby the first Slater integral is defined as $F_0 = U$, where U is the Hubbard repulsion, the Hund's rule coupling defined the other integrals via $J = (F_2 + F_4)/14$, and the ratio of F_4/F_2 is set to 0.625, typical for $3d$ transition metals [25]. We used $J = 0.9$ eV and varied U. The calculated total magnetization is $1.85\mu_B$/Fe without U and increases with U up to $2.17\mu_B$/Fe at $U = 3$ eV. As pointed out in Ref. [9], even at $U = 0$ eV this value is somewhat larger than in the experiment, which is quite common among metallic magnets (for instance, Fe-based superconductors or itinerant ferromagnets such as Ni_3Al). It is generally accepted that itinerant fluctuations, missing in the mean-field DFT approach, reduce the ordered moment [26].

Spin spiral and unrestricted noncollinear calculations were performed using the VASP package. For the former, the generalized Bloch theorem formalism [27] was utilized and verified against $1 \times 1 \times 4$ unrestricted noncollinear calculations. By construction, the spiral formalism does not include the spin-orbit coupling, but relevant energy differences were similar to those in relativistic supercell calculations.

Figure 2 summarizes the result of these calculations. We have scanned the irreducible part of the primitive Brillouin zone using the $5 \times 5 \times 4$ mesh with a step of $0.1G$ from the origin to $0.5G$ for each crystallographic direction (G are the corresponding reciprocal lattice vectors), altogether 216 calculations. One can see that the magnon spectrum is stiff along x and y and soft along z, with a minimum close to $\mathbf{q} = (0, 0, 0.27)$ in reciprocal lattice units. We then calculated the spiral energies with a finer mesh of $7 \times 7 \times 7$, along the line $\mathbf{q} = (0, 0, q_z)$, with a step of 0.02 in q_z (Fig. 2). The position of the minimum does not change. The value of $\mathbf{q} = (0, 0, 0.27)$ agrees well with the experimental number.

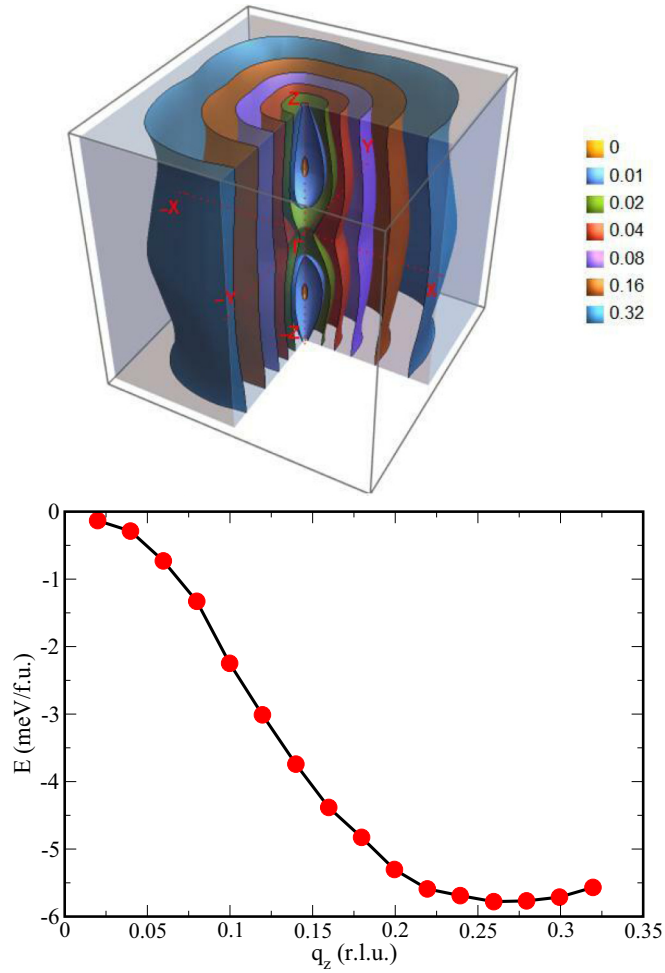

FIG. 2. Top: 3D contour plot of the total energy of a nonrelativistic spiral with a spiral vector $\mathbf{q} = (x, y, z)$, where x, y, z are components in reciprocal lattice coordinates. Bottom: the same for the vector $\mathbf{q} = (0, 0, z)$.

We have also tried to stabilize an amplitude SDW, as suggested in Ref. [14]. It never stabilizes, indicating that the DFT ground state is resoundingly spiral.

While the FM Fermi surface does not show any visible nesting feature and the noninteracting susceptibility (either χ_{zz} or χ_{+-}) does not show any well-defined maximum, the calculated density of states for the FM ($\mathbf{q} = 0$) and the spiral $\mathbf{q} = (0, 0, 0.27)$ states (Fig. 3)shows a small spectral weight transfer from the region within a few tenths of an eV near the Fermi level to farther energies, that is, a small, but noticeable, pseudogap effect. It is worth mentioning that looking at the nonmagnetic Fermi surface [14] is not very helpful since the

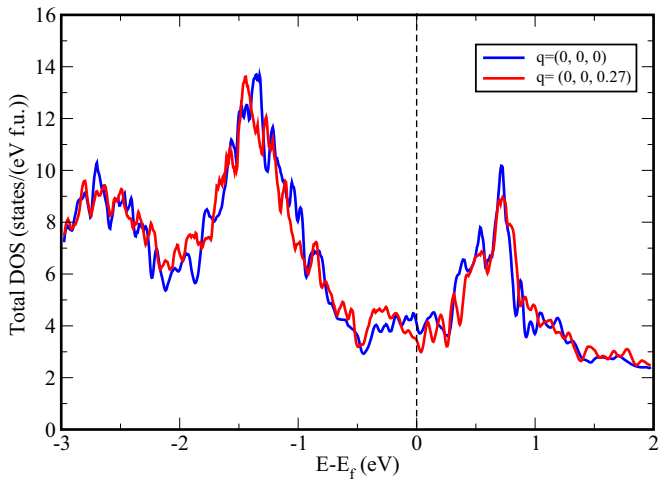

FIG. 3. Density of states near the Fermi level for the ferromagnetic [$\mathbf{q} = (0, 0, 0)$] and spiral [$\mathbf{q} = (0, 0, 0.27)$] states. Note small, but discernible, weight transfer away from the Fermi level.

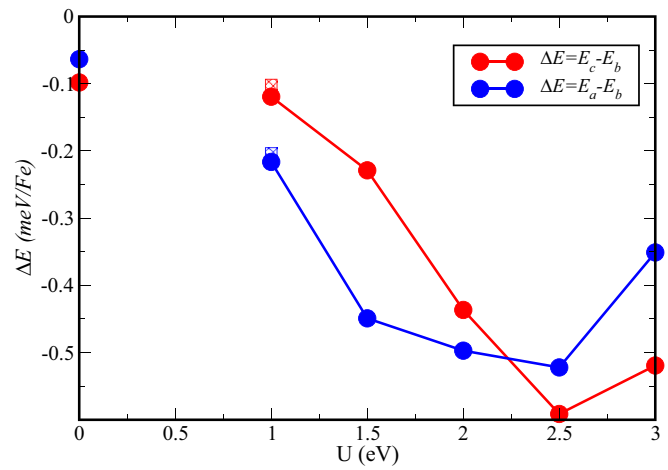

FIG. 4. Magnetoanisotropy energy for the quantization axis along the crystallographic a, b, and c axes. Calculations were performed in FPLO for Hund's rule coupling of $J = 0.9$ eV as a function of Hubbard U. Zero corresponds to DFT calculations without the GGA+U correction. The two points for $U = 1$ eV correspond to k-point meshes of $8 \times 8 \times 8$ and $12 \times 12 \times 12$.

SDW develops from the FM state and cannot be considered to be a small perturbation over the nonmagnetic state.

We have also calculated the magnetic anisotropy in the FM state as a function of the Hubbard correction U (calculations reported above did not include U). To this end, we used the FPLO method, which treats the relativistic effects more accurately, and the angular dependence of the GGA+U term is included in a more systematic way. The results are presented in Fig. 4. The calculated anisotropy is small and extremely sensitive to the computational setup. For instance, in the popular spherically symmetrized version of the LDA+U method [28] the calculations for $U = J$ are equivalent to no LDA+U correction at all, yet in our (unsymmetrized) calculations the results (the first two points in Fig. 4) are distinctly different. The calculation without the U correction and those with $U \geqslant 2.5$ eV agree with the experiment at $T < 60$ K. Those with $U \leqslant 2$ eV agree with the anisotropy derived for the susceptibility in the ASDW model at $T = 100$ K. Neither agrees with the anisotropy implied by the SS model.

TABLE I. Magnetic anisotropies as derived from the experiment [9,14] assuming the two models for the SDW phase and the results of the DFT calculations. χ indicates that the hierarchy is derived from the spin susceptibility data, and H_{flip} that from the spin-flip field values. See the main text for the details.

Temperature	Feature	Magnetic orientation
$T < 60$ K (Expt.)	χ, FM	$c < a, c < b$
$T = 100$ K (Expt.)	χ, ASDW	$a \ll c \lesssim b$
	χ, SS	$b \ll a \approx c$
	H_{flip}	$b \ll a \approx c$
$T = 0$ K (Calc.)	GGA	$c < a < b$
	GGA+$U \leqslant 2$ eV	$a < c < b$
	GGA+$U \geqslant 2.5$ eV	$c < a < b$

The main message is that the magnetic anisotropy is a very sensitive quantity to calculate, and theoretically, it is abnormally temperature dependent. The latter fact is often observed when a material includes inequivalent magnetic sites with opposite-sign local anisotropies and/or when a considerable part of the observed anisotropy comes not from the single site, but from exchange anisotropy. Neither of these two possibilities can be addressed by computational tools available to us. It is worth noting that an additional mechanism exists that can stabilize the helical spiral against either of the two possible cycloidal spirals and may be due to the dipole-dipole interaction [29]. Indeed, in the long-wavelength limit it contributes for

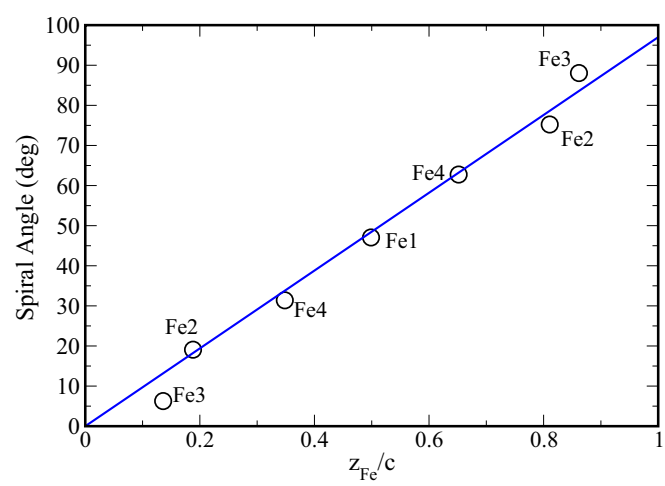

FIG. 5. Spiral angle as function of the position of an Fe layer within the unit cell for the spiral calculations with $\mathbf{q} = (0, 0, 0.27)$. No restrictions are imposed on the magnetic moment directions within a single unit cell, while the consecutive unit cells are rotated by $0.27 \times 360°$. The line shows the ideal sinusoid, $\alpha = 0.27 \times 360° z/c$.

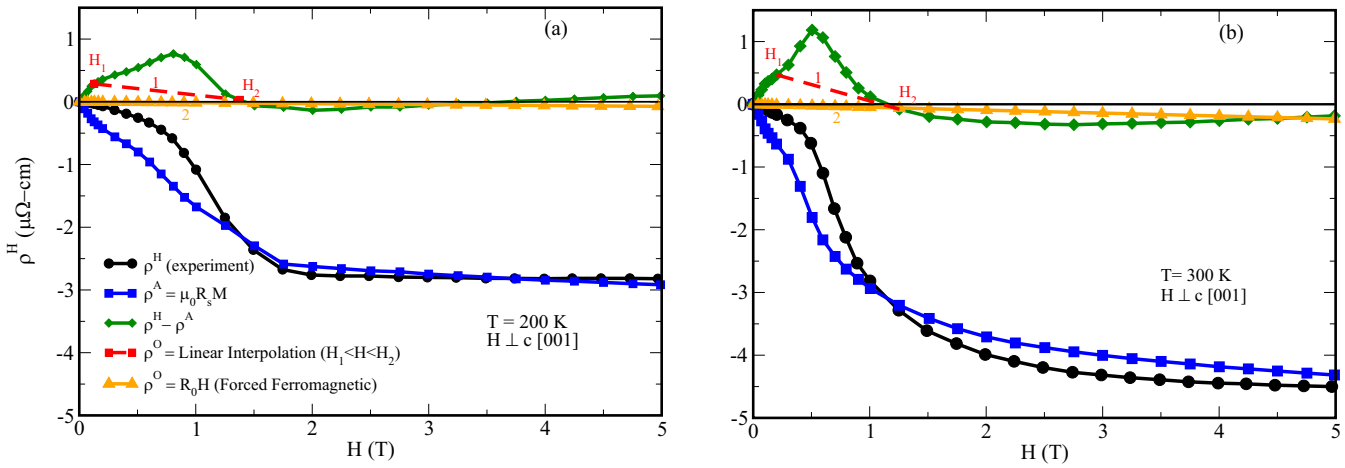

FIG. 6. Suggested decomposition of the Hall resistivity measured by Mendez *et al.* [9] for two different temperatures.

a cycloidal (but not helical) spiral an additional energy equal to $\int \pi m^2 dV$, where m is the magnetization density and the integration is over the entire crystal. Using the Fe_3Ga_4 parameters, we get an estimate of 0.06 meV/Fe, comparable with and slightly larger than the calculated (without U) electronic anisotropy energy. This mechanism can, in principle, explain why the condition $(E_a, E_b) < E_c$ may not be satisfied but the *ab* spiral may still be the ground state.

In principle, the next step would be to attempt to derive a first-principles Heisenberg Hamiltonian. In Fe_3Ga_4, unfortunately, it is virtually impossible because of too many inequivalent bonds and the fact that many ferrimagnetic configurations simply fail to converge. On the other hand, it appears that the SDW in Fe_3Ga_4 can be quite well described in a continuous model. Indeed, as discussed above, a unit cell includes nine Fe atoms arranged in seven separate *ab* Fe layers stacked along c. Our spin spiral calculations place no restriction on the mutual orientation of their magnetic moments. Yet the self-consistent solution can be very accurately described by a simple sinusoid, where the helix angle is given by $\alpha(z) = 0.27 \times 2\pi z/c$ (Fig. 5). Only the two Fe3 (see Fig. 1) layers slightly deviate from this formula.

Interestingly, the calculated energy as a function of the spiral vector is very well described by the function

$$E = E_0 + J_1 \cos 2\pi qh + J_2 \cos 4\pi qh, \tag{3}$$

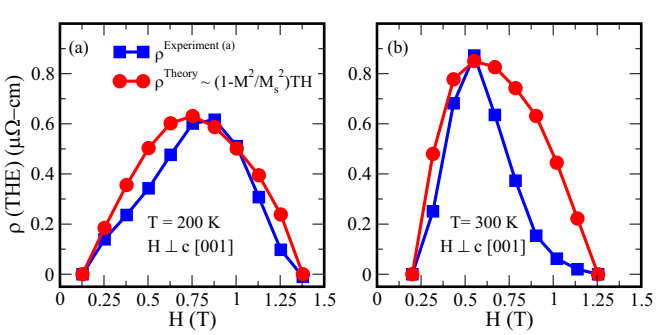

FIG. 7. Topological Hall effect resistivity extracted as described in the text compared to Eq. (7).

where $h = 1.75$, $J_1 = 3$ meV, and $J_2 = 0.4$ meV, as if the Hamiltonian were composed of two antiferromagnetic Heisenberg interactions, one acting across a distance of $1.75c$ and the other acting across a distance of $3.5c$. Of course, in reality this would be only an effective Hamiltonian, resulting from concerted action of all sorts of exchange interactions, but it indicates that the overall magnetic coupling is extremely long range.

In any event, the calculations unambiguously indicate that of the two possible ground states compatible with the neutron scattering data it is the helical spiral that is realized and not an ASDW.

IV. TOPOLOGICAL HALL EFFECT

Typically, the Hall effect in metals is described as a sum of two components: the ordinary Hall effect [30], stemming from the Lorentz force experienced by the charge carriers, and the anomalous Hall effect [30], resulting from the interplay between the exchange field and spin-orbit coupling. While there are notable exceptions (in particular, the anomalous Hall effect was shown to exist even in some systems with zero magnetization [6]), it is customary to assume that the ordinary Hall resistance is proportional to the applied field, $\rho^O = R_0 H$, and the anomalous one is proportional to the net magnetization, $\rho^A = R_s M$. Recently, it was pointed out that in noncoplanar magnets a third term should be added (see, for instance, Ref. [7]), called the topological Hall effect, proportional to the so-called scalar spin chirality s, which can be defined in a discrete representation as a triangular loop over near-neighbor magnetic moment, $s = \mathbf{M}_1 \cdot (\mathbf{M}_2 \times \mathbf{M}_3)$.

In the continuous representation one can define the topological field,

$$b_i(\mathbf{r}) = \sum_{jk} e_{ijk} \mathbf{M}(\mathbf{r}) \cdot \left(\frac{\partial \mathbf{M}(\mathbf{r})}{\partial r_i} \times \frac{\partial \mathbf{M}(\mathbf{r})}{\partial r_k} \right) \tag{4}$$

$$= \sum_{jk} \sum_{\alpha\beta\gamma} e_{ijk} e_{\alpha\beta\gamma} M_\alpha \frac{\partial M_\beta}{\partial r_i} \frac{\partial M_\gamma}{\partial r_k}, \tag{5}$$

where i, j, and k are Cartesian indices in real space and α, β, and γ in spin space. This field can couple with the external

magnetic field and generate an additional contribution to the Hall resistivity in the field parallel to **b** [7]. As a result, the Hall resistivity is commonly written as

$$\rho^H = R_0 H + R_s M + \rho^T. \tag{6}$$

It is well known that a nonzero topological field **b** can be generated by a linear combination of three (but not two) helical spirals [31]. It was recently pointed out [10] that a combination of two spirals, where one is helical and the other is transverse conical, can have a nonzero topological field. Furthermore, Ghimire *et al.* [10] argued that even if the ground state is a *single* helical spiral propagating along a given direction, say, z, in a suitable magnetic field $\mathbf{H}||\mathbf{x} \perp \mathbf{z}$, this spiral is liable to flop into a transverse conical spiral, propagating along z and canted toward x. Furthermore, it was also shown [10] that spin fluctuations in the form of a helical magnon propagating along y can be selectively excited, generating a topological field (and hence the topological Hall effect) proportional to the temperature and also dependent on the net magnetization. In Ref. [10] a simple formula was derived which reads

$$\rho^T = \kappa(1 - M^2/M_s^2)TH, \tag{7}$$

where κ is an unknown, material-specific constant and M_s is the saturation magnetization.

However, direct substitution of Eq. (7) into Eq. (6) is not possible because the assumption that R_0 and R_s do not depend on magnetic field is, while popular, generally incorrect. Both coefficients are determined by the electronic structure, which, in turn, is very sensitive to magnetic order. This problem was discussed in Ref. [10], where the following protocol was worked out: First, the Hall resistivities in the nontopological phases below (in terms of the external field H) or above the topological phase ($H_1 < H < H_2$) are fit separately to the first two terms in Eq. (6). In principle, they should then be continuously connected to each other across the topological region and subtracted from the total ρ^H. In Ref. [10], for the lack of any justifiable recipe, they were simply connected by a straight line. Now, since the difference, which we will call ρ^T, is, by construction, zero at H_1 and H_2, they subtracted the linear base $\rho_0 = [(H - H_1)\rho^T(H_2) + (H_2 - H)\rho^T(H_1)]/(H_2 - H_1)$, where $\rho^T(H)$ was taken from Eq. (7).

We have followed this protocol, although the experimental data are not nearly as clean as in YMn_6Sn_6 (Fe_3Ga_4 is known to form with considerable disorder); in particular, proper identification of the first and second spin-flop fields is difficult. Still, we were able to tentatively assign them to be (see Fig. 6) at $T = 200$ K, $H_1 \approx 0.125$ T, and $H_2 \approx 1.375$ T and at $T = 300$ K, $H_1 \approx 0.18$ T, and $H_2 \approx 1.25$ T (at lower temperatures the topological signal is too weak to analyze quantitatively). The results of this analysis are shown in Fig. 7. Note that the amplitude of the topological signal is about 40% higher at $T = 300$ K, in good agreement with $300/200 = 1.5$, consistent with the linear dependence on T in Eq. (7).

V. CONCLUSIONS

We have studied, using density functional theory, the magnetic properties of a potential topological Hall material, Fe_3Ga_4 metal. We found that the DFT ground state is a spin spiral, propagating along the crystallographic c direction with $\mathbf{q} = (0, 0, 0.27)$ reciprocal lattice units. This is in excellent agreement with the neutron scattering findings for temperatures above ~100 K. Contrary to the previously published conjecture, we identified this state as a spiral, not an amplitude spin density wave. We argue that the actual ground state, despite b being (slightly) the hard magnetic axis, is an *ab* helical spiral, stabilized by dipole-dipole interactions.

We have further identified a spin-flop field at which the helical spiral flops into a transverse conical spiral, according to the theory proposed recently by one of us for another topological Hall spiral magnet, YMn_6Sn_6. The same theory works well for Fe_3Ga_4. Indeed, the theory predicts a topological Hall effect in only the transverse conical phase, with a strong (approximately linear) temperature dependence, and both predictions are corroborated by the experiment. This second observation of the dynamically fluctuation-induced topological Hall effect strongly suggests that the proposed theory is correct and sufficiently universal.

ACKNOWLEDGMENTS

The authors acknowledge funding from the U.S. Department of Energy through Grant No. DE-SC0021089. We also acknowledge the Department of Defense (DOD) Major Shared Computing Resource Center at Air Force Research Laboratory (AFRL) and the National Energy Research Scientific Computing Center (NERSC) for high-performance computing facilities, where some portions of the calculations were performed. Last, but not least, we acknowledge many insightful discussions with M. Mostovoy. The authors are particularly grateful to H. Cao for discussions and careful reading of the revised version of this paper.

[1] *Topology in Magnetism*, edited by J. Zang, V. Cros, and A. Hofmann (Springer, Berlin, 2018).

[2] N. Nagaosa and Y. Tokura, Topological properties and dynamics of magnetic skyrmions, Nat. Nanotechnol. **8**, 899 (2013).

[3] N. Nagaosa, X. Z. Yu, and Y. Tokura, Gauge fields in real and momentum spaces in magnets: Monopoles and skyrmions, Philos. Trans. R. Soc. A **370**, 5806 (2012).

[4] B. Bradlyn, J. Cano, Z. Wang, M. G. Vergniory, C. Felser, R. J. Cava, and B. A. Bernevig, Beyond Dirac and Weyl fermions: Unconventional quasiparticles in conventional crystals, Science **353**, aaf5037 (2016).

[5] N. P. Armitage, E. J. Mele, and A. Vishwanath, Weyl and Dirac semimetals in three-dimensional solids, Rev. Mod. Phys. **90**, 015001 (2018).

[6] L. Ŝmejkal, R. Gonźalez-Herńandez, T. Jungwirth, and J. Sinova, Crystal time-reversal symmetry breaking and sponta-

neous Hall effect in collinear antiferromagnets, Sci. Adv. **6**, eaaz8809 (2020).

[7] P. Bruno, V. K. Dugaev, and M. Taillefumier, Topological Hall Effect and Berry Phase in Magnetic Nanostructures, Phys. Rev. Lett. **93**, 096806 (2004).

[8] S. S. Zhang, H. Ishizuka, H. Zhang, G. B. Halász, and C. D. Batista, Real-space Berry curvature of itinerant electron systems with spin-orbit interaction, Phys. Rev. B **101**, 024420 (2020).

[9] J. H. Mendez, C. E. Ekuma, Y. Wu, B. W. Fulfer, J. C. Prestigiacomo, W. A. Shelton, M. Jarrell, J. Moreno, D. P. Young, P. W. Adams, A. Karki, R. Jin, J. Y. Chan, and J. F. DiTusa, Competing magnetic states, disorder, and the magnetic character of Fe_3Ga_4, Phys. Rev. B **91**, 144409 (2015).

[10] N. J. Ghimire, R. L. Dally, L. Poudel, D. C. Jones, D. Michel, N. Thapa Magar, M. Bleuel, M. A. McGuire, J. S. Jiang, J. F. Mitchell, J. W. Lynn, and I. I. Mazin, Competing magnetic phases and fluctuation-driven scalar spin chirality in the kagome metal YMn_6Sn_6, Sci. Adv. **6**, eabe2680 (2020).

[11] G. Gong, L. Xu, Y. Bai, Y. Wang, S. Yuan, Y. Liu, and Z. Tian, Large topological Hall effect near room temperature in noncollinear ferromagnet $LaMn_2Ge_2$ single crystal, Phys. Rev. Mater. **5**, 034405 (2021).

[12] Q. Wang, K. J. Neubauer, Ch. Duan, Q. Yin, S. Fujitsu, H. Hosono, F. Ye, R. Zhang, S. Chi, K. Krycka, H. Lei, and P. Dai, Field-induced topological Hall effect and double-fan spin structure with a *c*-axis component in the metallic kagome antiferromagnetic compound YMn_6Sn_6, Phys. Rev. B **103**, 014416 (2021).

[13] I. I. Mazin and J. Schmalian, Pairing Symmetry and pairing state in ferropnictides: Theoretical overview, Phys. C (Amsterdam, Neth.) **469**, 614 (2009).

[14] Y. Wu, Z. Ning, H. Cao, G. Cao, K. A. Benavides, S. Karna, G. T. McCandless, R. Jin, J. Y. Chan, W. A. Shelton, and J. F. DiTusa, Spin density wave instability in a ferromagnet, Sci. Rep. **8**, 5225 (2018).

[15] K. Momma and F. Izumi, VESTA-3 for three-dimensional visualization of crystal, volumetric and morphology data, J. Appl. Crystallogr. **44**, 1272 (2011).

[16] H. Cao (Private communication).

[17] G. Kresse and J. Hafner, *Ab initio* molecular dynamics for liquid metals, Phys. Rev. B **47**, 558 (1993).

[18] G. Kresse and J. Hafner, *Ab initio* molecular-dynamics simulation of the liquid-metal-amorphous-semiconductor transition in germanium, Phys. Rev. B **49**, 14251 (1994).

[19] G. Kresse and J. Furthmuller, Efficient iterative schemes for *ab initio* total-energy calculations using a plane-wave basis set, Phys. Rev. B **54**, 11169 (1996).

[20] G. Kresse and J. Furthmuller, Efficiency of ab-initio total energy calculations for metals and semiconductors using a plane-wave basis set, Comput. Mater. Sci. **6**, 15 (1996).

[21] J. P. Perdew, K. Burke, and M. Ernzerhof, Generalized Gradient Approximation Made Simple, Phys. Rev. Lett. **77**, 3865 (1996).

[22] K. Koepernik and H. Eschrig, Full-potential nonorthogonal local-orbital minimum-basis band-structure scheme, Phys. Rev. B **59**, 1743 (1999); FPLO, http://www.fplo.de.

[23] H. Eschrig, M. Richter, and I. Opahle, Relativistic Solid State-Calculations, in *Relativistic Electronic Structure Theory. Part II: Applications*, edited by P. Schwerdtfeger (Elsevier, Amsterdam, 2004), vol. 14, pp. 723–776.

[24] E. R. Ylvisaker, W. E. Pickett, and K. Koepernik, Anisotropy and magnetism in the LSDA+U method, Phys. Rev. B **79**, 035103 (2009).

[25] V. I. Anisimov, I. V. Solovyev, M. A. Korotin, M. T. Czyzyk, and G. A. Sawatzky, Density-functional theory and NiO photoemission spectra, Phys. Rev. B **48**, 16929 (1993).

[26] T. Moriya, *Spin Fluctuations in Itinerant Electron Magnetism*, Solid State Sciences, Vol. 56, (Springer, Berlin, 1985).

[27] L. M. Sandratskii, Energy band structure calculations for crystals with spiral magnetic structure, Phys. Status Solidi B **136**, 167 (1986).

[28] S. L. Dudarev, G. A. Botton, S. Y. Savrasov, C. J. Humphreys, and A. P. Sutton, Electron-energy-loss spectra and the structural stability of nickel oxide: An LSDA+U study, Phys. Rev. B **57**, 1505 (1998).

[29] We thank M. Mostovoy for pointing this possibility out to us.

[30] C. M. Hurd, *The Hall Effect in Metals and Alloys*, International Cryogenics Monograph Series (Plenum, New York, 1972).

[31] S. Mühlbauer, B. Binz, F. Jonietz, C. Pfleiderer, A. Rosch, A. Neubauer, R. Georgii, and P. Böni, Skyrmion lattice in a chiral magnet, Science **323**, 915 (2009).